International Journal of Mechanical, Industrial and Aerospace Sciences
ISSN: 2517-9950
Vol:6, No:3, 2012

Numerical Analysis of Laminar to Turbulent Transition on the DU91-W2-250 airfoil

M. Raciti Castelli, G. Grandi and E. Benini

***Abstract*—**This paper presents a study of laminar to turbulent transition on a profile specifically designed for wind turbine blades, the DU91-W2-250, which belongs to a class of wind turbine dedicated airfoils, developed by Delft University of Technology. A comparison between the experimental behavior of the airfoil studied at Delft wind tunnel and the numerical predictions of the commercial CFD solver ANSYS FLUENT® has been performed. The prediction capabilities of the Spalart-Allmaras turbulence model and of the γ-θ Transitional model have been tested. A sensitivity analysis of the numerical results to the spatial domain discretization has also been performed using four different computational grids, which have been created using the mesher GAMBIT®.

The comparison between experimental measurements and CFD results have allowed to determine the importance of the numerical prediction of the laminar to turbulent transition, in order not to overestimate airfoil friction drag due to a fully turbulent-regime flow computation.

***Keywords*—**CFD, wind turbine, DU91-W2-250, laminar to turbulent transition

I. Introduction and Background

With its 2020 goals to increase the share of renewable energy in the overall energy mix to 20% and to cut carbon emissions by 20%, the EU is leading the world in terms of renewable energy deployment, exports and promotion. Today Europe gets approximately 20% of its electricity from renewable energy sources, including 5.3% from wind Energy. That share will increase up to 2020 when, under the terms of the EU's renewable energy directive, which sets legally binding targets for renewable energy in Europe, 34% of the EU's total electricity consumption will come from renewable energy sources, with wind energy accounting for 14% [1]. In this scenario, the continuous quest for clean energy appears to be connected with the development of the aerodynamics of actual wind turbines, in order to achieve a growth of their performances, both for the classical horizontal-axis (HAWT) and also the vertical-axis (VAWT) concepts [2].

For the past years, it was common practice to use existing airfoil families, like the well known NACA series, for the design of wind turbine blades, however the need of furthering wind turbine technologies has led to the quest for alternatives.

Marco Raciti Castelli is a Research Associate at the Department of Industrial Engineering of the University of Padua, Via Venezia 1, 35131 Padua, Italy (e-mail: marco.raciticastelli@unipd.it).

Giada Grandi is a M.Sc. student in Aerospace Engineering at the University of Padua, Via Venezia 1, 35131 Padua, Italy.

Ernesto Benini is Associate Professor at the Department of Industrial Engineering of the University of Padua, Via Venezia 1, 35131 Padua, Italy (e-mail: ernesto.benini@unipd.it).

The airfoil analyzed in the present work is the DU91-W2-250, which belongs to a class of wind turbine dedicated airfoils developed by Delft University of Technology. At present, DU airfoils are being used by various wind turbine manufacturers worldwide, in many different rotor blades.

The design of the DU91-W2-250 airfoil followed wind tunnel tests on a 25% thick NACA airfoil from the 63-4xx series, linearly scaled from 21%. To compensate for the resulting loss in lift of the upper surface, a certain amount of lower surface aft loading was incorporated, giving DU91-W2-250 the typical S-shape of the pressure side. This airfoil, like other 25% thick airfoils, has very high peak lift coefficient in the smooth condition and presents an acceptable performance in the rough situation, differently from classical NACA airfoils. The main features of the mid span airfoil are a good maximum lift to drag ratio and a smooth stall behavior [3] [4].

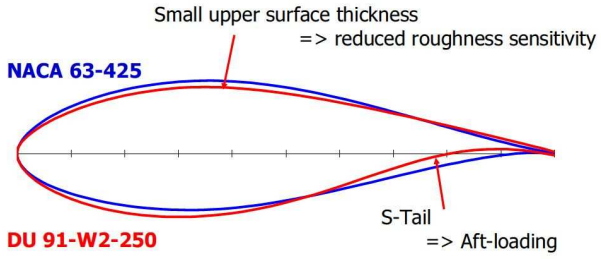

Fig.1 Comparison between the DU91-W2-250 airfoil and a 5-digit NACA airfoil

Every flow causes pressure and friction on the body surface, which result in forces and moments acting on the body itself. Nowadays, thanks to advances in numerical methods and computing power, the investigation and solution of the flow field around an airfoil has become relatively simple. By performing CFD analysis on the DU91-W2-250, together with turbulence and transition modeling testing, the main purpose of the present work is to investigate its behavior, with particular attention to the laminar to turbulent transition phenomena.

Lombardi et al. [5] tested the capability of a classical RANS solver of predicting the friction drag over a NACA 0012 airfoil for 0 deg angle of attack and compared CFD results with the values given by a coupled potential/boundary-layer method. The analyzed range of Reynolds numbers varied from 300,000 to 9,000,000. As a result, being the local skin friction coefficient defined as:

$$c_f = \tau_w / (\tfrac{1}{2}\cdot\rho\cdot c\cdot V_\infty^2) \quad (1)$$

the relative integral over the whole airfoil length resulted overestimated by all turbulence models - even using highly refined grids - because of their inherent inability to predict the boundary layer transition.

Lian and Shyy [6] coupled a Navier-Stokes solver and a Reynolds-averaged two-equation closure to study laminar to turbulent transition for low Reynolds number flows around a SD7003 airfoil, obtaining good agreement between numerical predictions and experimental measurements regarding the transition location, as well as overall flow structures.

Menter et al. [7], [8] developed the γ-θ model, one of the first transition prediction tools available in a commercial flow solver, which is compatible with modern CFD approaches. The model is based on two transport equations, one for intermittency and one for the transition onset criteria in terms of momentum thickness Reynolds number. A significant number of test cases were used to validate the transition model for turbomachinery and aerodynamic applications, including a 2D horizontal-axis wind turbine airfoil section [8].

Benini and Ponza [9] investigated the capability of the γ-θ transition model in predicting the laminar to turbulent transition in the boundary layer developing around a supercritical airfoil (NLR 7301). The numerical results showed a certain degree of sensitivity to the turbulence intensity level set at the domain inlet, being the transition onset moved foreward with increasing turbulence levels.

Hosseinverdi and Boroomand tested the capability of two empirical correlations (Cebeci & Smith and e^N method) coupled to the two-equation k-ω SST turbulence model of Menter, in order to predict the incompressible transitional flow over a S809 wind turbine airfoil, obtaining significant improvements in drag prediction by using the transitional computation in comparison with the fully turbulent simulation [10].

Yuhong and Congming [11] applied a two-equation transition model to the flow over a wind turbine S814 airfoil. Numerical predictions were compared with the experimental data of the National Renewable Energy Laboratory (NREL) and the simulation results using fully turbulent SST model. The analysis showed that the transition model can capture the phenomena of transition and flow separation more effectively. Under certain working conditions, the transition model resulted able to predict lift and drag coefficients more accurately than a full turbulence model.

The main objective of this work is a 2D numerical investigation on DU91-W2-250 airfoil, performed to demonstrate how, using a numerical tool capable to foresee the laminar to turbulent transition, it is possible to avoid numerical results being affected by the overestimation of airfoil friction drag due to a fully turbulent-regime flow computation. The proposed analysis focuses mainly on three parameters:

- aerodynamic coefficients C_l, C_d ;
- the wall y^+ ;
- skin friction coefficient c_f.

The reference values for the considered airfoil derived from measurements performed at Delft University Low-speed Wind Tunnel [12] at a Reynolds number of 3.0×10^6, which is typical for wind turbine applications. In this case, laminar to turbulent free transition (it is assumed that the smooth surface does not trigger turbulence until the laminar boundary layer becomes unstable and the flow experiences free transition to turbulence) is an important factor to be taken into account. Table I summarizes the main reference values of the experimental tests.

TABLE I
MAIN REFERENCE VALUES OF THE EXPERIMENTAL MEASUREMENTS

Denomination	Value
Airfoil section	DU91-W2-250
c [m]	0.6
Re [-]	$3.0\cdot10^6$
α [deg]	0.49

CFD analysis was performed using both Spalart-Allmaras turbulence model and γ-θ Transitional model. The first one is a relatively simple one-equation model that solves a modeled transport equation for the kinematic eddy viscosity; this model was designed specifically for aerospace applications involving wall-bounded flows and was shown to give good results for boundary layers subjected to adverse pressure gradients [13].

The second one is based on the coupling of the SST transport equations with two other transport equations, one for the intermittency and one for the transition onset criteria, in terms of momentum-thickness Reynolds number [7] [8]. Its main characteristic is, however, the capability of foreseeing laminar to turbulent transition. In fact, classical turbulence models, although widely used to calculate the pressure loads acting on blade profiles, are unable to predict the laminar-turbulent transition, resulting in poor prediction of rotor performance, caused by the overestimation of airfoil friction drag due to a fully turbulent-regime flow computation [14], especially for high values of the tip speed ratio where, due to the low range of blade relative angles of attack, the skin friction contribution to overall airfoil drag is quite relevant [15].

II. Model Geometry

The present work was performed applying both Spalart-Allmaras turbulence model and γ-θ Transitional model to four different spatial domain discretizations created with the mesher GAMBIT®. The grids were substantially constructed in the same way, differing from each other by the number of layers which composed the near-wall discretization. The computational domain was in fact subdivided in two sub-domains:

- an external portion, comprising the whole simulation domain;
- an internal portion, bounding the area close to the airfoil section. Great attention was directed to this element: in fact, the most important differences between the four proposed meshes were concentrated in it.

A high-quality mesh was created close to the airfoil surface with the purpose of better capturing the surface boundary layer and to obtain y^+ values close to 1. This parameter is a mesh-

dependent dimensionless distance that quantifies the degree of wall layer resolution, in formulas:

$$y^+ = (\rho \cdot u_\tau \cdot y) / \mu \quad (2)$$

Each grid was called as "Mod" followed by a number from 1 to 4. Tables II and III summarize the main features of the adopted grids, as well as the resulting y^+ peak values.

TABLE II
MAIN MESH FEATURES AND Y^+ VALUES OBTAINED USING THE SPALART-ALLMARAS TURBULENCE MODEL

Name	First row [mm]	Growth factor [-]	Rows [-]	Suction side peak y^+ value [-]	Pressure side peak y^+ value [-]
Mod1	0.7	1.2	4	110	110
Mod2	0.05	1.2	15	7.5	7
Mod3	0.025	1.2	17	3.8	3.5
Mod4	0.0125	1.2	21	1.85	1.8

TABLE III
MAIN MESH FEATURES AND Y^+ VALUES OBTAINED USING THE Γ-Θ TRANSITIONAL MODEL MODEL

Name	First row [mm]	Growth factor [-]	Rows [-]	Suction side peak y^+ value [-]	Pressure side peak y^+ value [-]
Mod1	0.7	1.2	4	110	105
Mod2	0.05	1.2	15	8.25	8.5
Mod3	0.025	1.2	17	3.5	3
Mod4	0.0125	1.2	21	1.8	1.6

III. DESCRIPTION OF THE NUMERICAL FLOW FIELD

As already mentioned in the previous section, all the adopted grids presented common geometric features, except for the areas close to the airfoil. As the aim of the numerical simulations was to explore the 2D flow field close to a blade profile, the computational domain was discretized into two macro-areas:

- a rectangular outer zone, determining the overall calculation domain, with a circular opening centered at 25% of chord length, which was identified as *Wind Tunnel sub-grid*, fixed;
- a circular inner zone, which was identified as *Airfoil sub-grid*, were grid points were clustered in order to obtain an accurate mesh setup of both the wall boundary layer and the airfoil wake.

Fig. 2 shows the main dimensions and boundary conditions of the *Wind Tunnel sub-grid* area. The computational domain width was set to 20 blade chords. In order to allow a full development of the wake behind the airfoil, inlet and outlet boundary conditions were placed respectively 10 blade chord upwind and 20 blade chord downwind with respect to the airfoil test section.

Two *symmetry* boundary conditions were used for the two side walls. The boundary between *Wind Tunnel sub-grid* and *Airfoil sub-grid* was set as an *interior*, thus ensuring the continuity of the flow field.

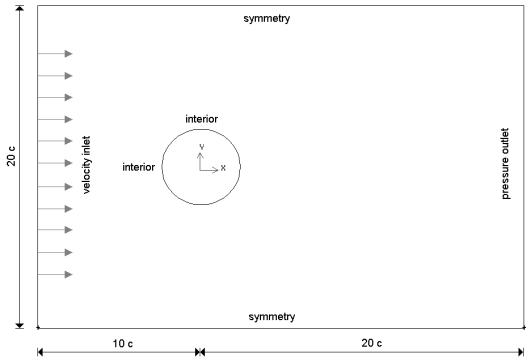

Fig. 2 Main dimensions and boundary conditions of the *Wind Tunnel sub-grid* area

TABLE IV
MAIN REFERENCE VALUES OF THE NUMERICAL FLOW FIELD

Denomination	Value
ρ [kg/m3]	1.225
μ [Pa·s]	$1.7894 \cdot 10^{-5}$
V_x [m/s]	73
V_y [m/s]	0

IV. DISCRETIZATION OF THE NUMERICAL FLOW FIELD

A totally unstructured mesh was chosen for the *Wind Tunnel sub-grid*, in order to reduce the engineering time to prepare the CFD simulations.

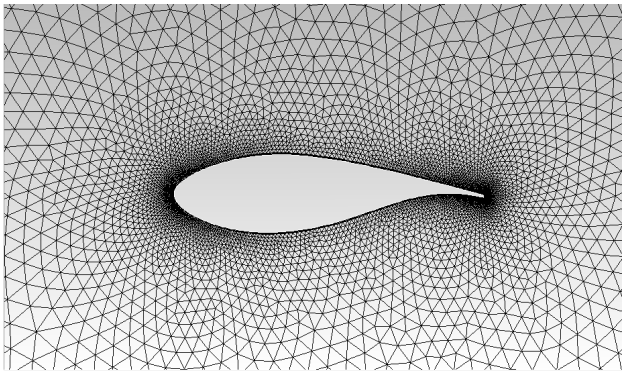

Fig. 3 *Airfoil sub-grid* mesh, Mod 1

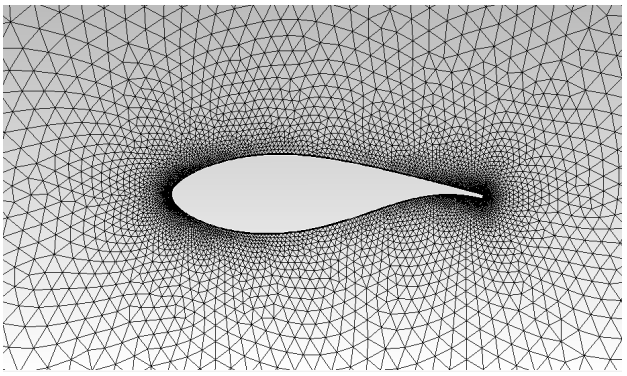

Fig. 4 *Airfoil sub-grid* mesh, Mod 2

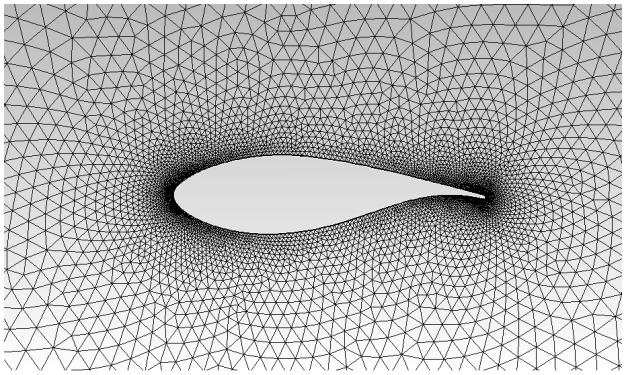
Fig. 5 *Airfoil sub-grid mesh*, Mod 3

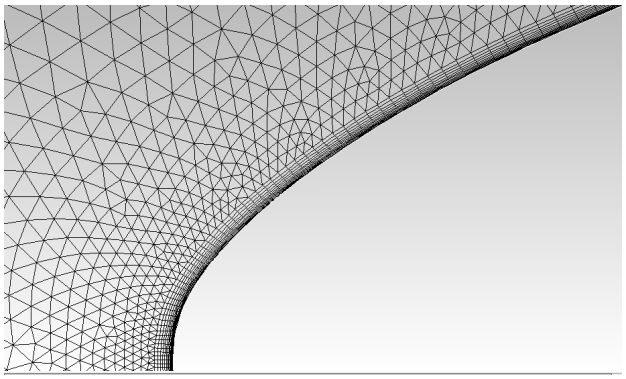
Fig. 6 Leading edge details of *Airfoil sub-grid mesh*, Mod 3

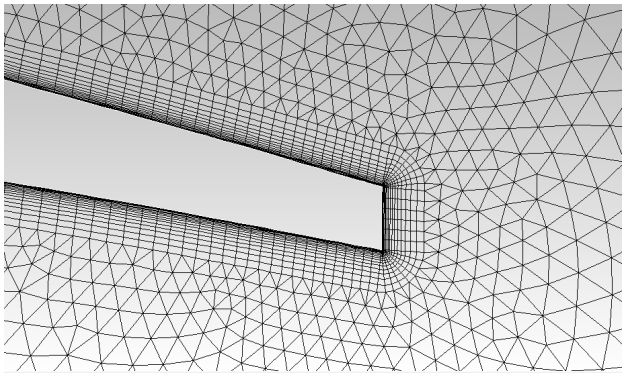
Fig. 7 Trailing edge details of *Airfoil sub-grid mesh*, Mod 3

With regard to the *Airfoil sub-grid*, the computational grids around the tested airfoil were constructed from lower topologies to higher ones, adopting appropriate size functions, in order to cluster grid points near the leading edge and the trailing edge of the blade profile, so as to improve the CFD code capability of determining lift, drag and the laminar to turbulent transition onset.

A high-quality structured mesh was created close to the airfoil surface, in order to better capture the boundary layer, while outside the boundary layer region a triangular unstructured grid was created using proper size functions. Figs. from 3 to 8 show the main features of the computational grids around the tested airfoil for the four candidate meshes. Some details of the grid close to the leading and trailing edge are also shown for Mod 3 mesh.

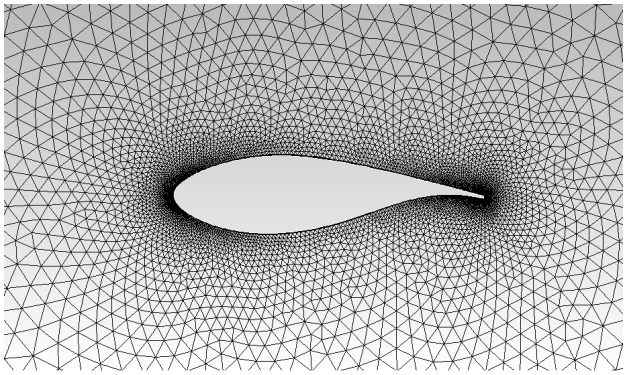
Fig. 8 Airfoil sub-grid mesh, Mod 4

V. Simulated Flow Conditions

Simulations were performed using the commercial RANS solver ANSYS FLUENT®, which implements 2-D Reynolds-averaged Navier-Stokes equations using a finite volume-finite element based solver. A segregated solver, implicit formulation, was chosen for unsteady flow computation. The fluid was assumed to be incompressible. As a global convergence criterion, residuals were set to 10^{-5}.

VI. Results and Discussion

Table V shows the DU91-W2-250 reference lift and drag values, respectively defined as:

$$C_l = L / (½\cdot\rho\cdot c\cdot V_\infty^2) \quad (3)$$

$$C_d = D / (½\cdot\rho\cdot c\cdot V_\infty^2) \quad (4)$$

which were measured at Delft University Low-speed Wind Tunnel [12] for an angle of attack of $\alpha = 0.49$ deg.

TABLE V
DU91-W2-250 reference lift and drag values measured at Delft University Low-speed Wind Tunnel for a = 0.49 deg (from: [12])

Denomination	Value
Cl [-]	0.469
Cd [-]	0.00766

TABLE VI
Numerical predicted lift coefficient and relative percentage deviation with respect to experimental measurements, Spalart-Allmaras turbulence model

Denomination	C_l [-]	C_d [-]
Mod1	0.38176 (-18.6%)	0.01558 (+103.3%)
Mod2	0.42409 (-9.6%)	0.01298 (+69.5%)
Mod3	0.42691 (-9%)	0.01307 (+70.6%)
Mod4	0.42211 (-10%)	0.01331 (+73.8%)

Tables VI and VII show a comparison between computed and measured lift and drag coefficients, as a function of the adopted spatial discretization, for both Spalart-Allmaras turbulence model and γ-θ Transitional model. It clearly appears that Mod 3 and Mod4 grids determine the best results in terms of percentage deviations from the experimental measurements. Moreover, the prediction capabilities of the γ-θ Transitional model appear to be quite higher with respect to the Spalart-Allmaras turbulence model, as far as drag prediction is concerned.

TABLE VII
NUMERICAL PREDICTED LIFT COEFFICIENT AND RELATIVE PERCENTAGE DEVIATION WITH RESPECT TO EXPERIMENTAL MEASUREMENTS, Γ-Θ TRANSITIONAL MODEL

Denomination	C_l [-]	C_d [-]
Mod1	0.31888 (-32%)	0.01633 (+113.3%)
Mod2	0.3367 (-28.3%)	0.01409 (+83.9%)
Mod3	0.44596 (-4.9%)	0.00886 (+15.7%)
Mod4	0.44381 (-5.4%)	0.00908 (+18.5%)

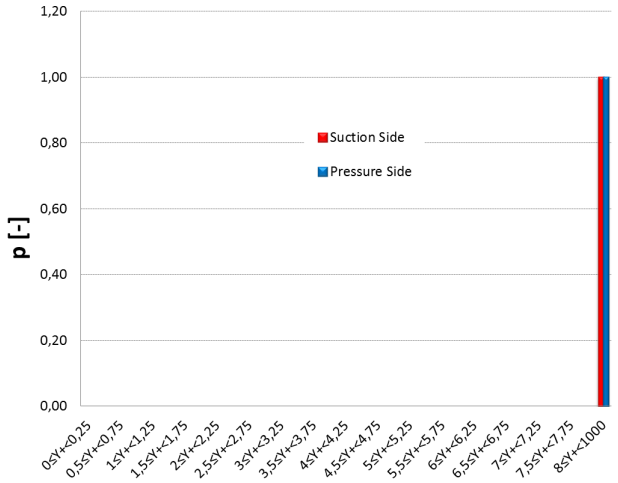

Fig. 9 Graphical representation of the distribution of the y^+ parameter along blade pressure and suction sides; Mod1 mesh, Spalart-Allmaras turbulence model

Figs. from 9 to 16 show the distribution of the y^+ parameter along both airfoil pressure and suction sides for the four candidate grid architectures.

A statistical procedure was created with the aim of determining the optimal distribution of the y^+ along the airfoil: a global interval [0;1000] was considered for the y^+ parameter, then the sub-interval [0;8] was subdivided into a series of steps of 0.25, while all values between 8 and 1000 were picked up together.

The probability for the y^+ value, at any given point along the airfoil, to be comprised inside each sub-interval was defined as:

$$p = Y/X \quad (5)$$

being X the number of grid elements having the y^+ comprised in the considered interval and Y the total number of grid elements on airfoil pressure/suction side.

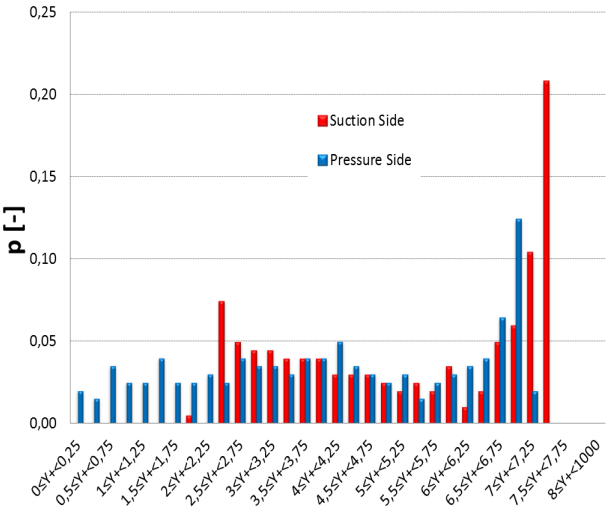

Fig. 10 Graphical representation of the distribution of the y^+ parameter along blade pressure and suction sides; Mod2 mesh, Spalart-Allmaras turbulence model

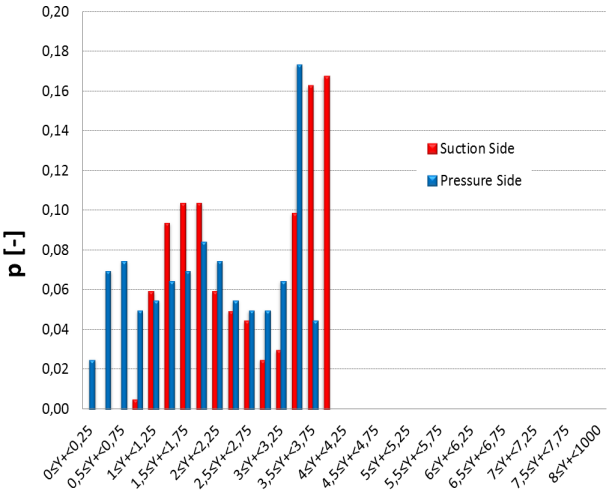

Fig. 11 Graphical representation of the distribution of the y^+ parameter along blade pressure and suction sides; Mod3 mesh, Spalart-Allmaras turbulence model

The higher quality of Mod 3 grid spacing, confirmed by the good results obtained by the computation of the aerodynamic coefficients, clearly appears from the distribution of the relative y^+ parameter between the prescribed values $1 \leq y^+ \leq 5$. The use of the proposed statistical methodology for the analysis of the quality of the grid is independent from the tested airfoil geometry or angle of attack and could be generalized for the whole polar of the considered airfoil.

Further work should be performed, in order to numerically determine the whole range of lift and drag coefficients for the considered airfoil geometry, as a function of the angle of attack.

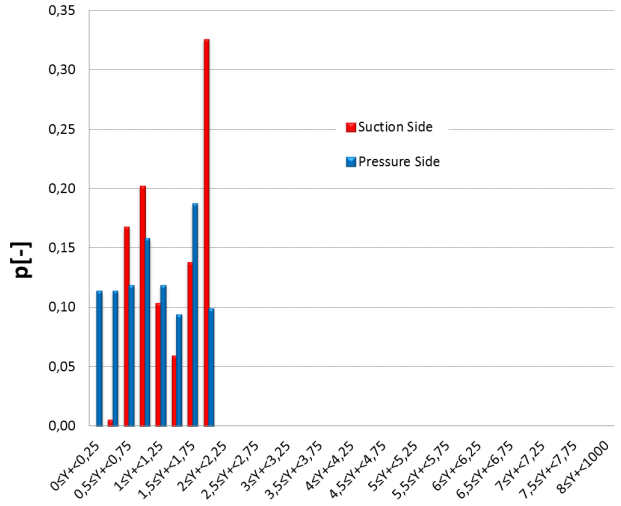

Fig. 12 Graphical representation of the distribution of the y^+ parameter along blade pressure and suction sides; Mod4 mesh, Spalart-Allmaras turbulence model

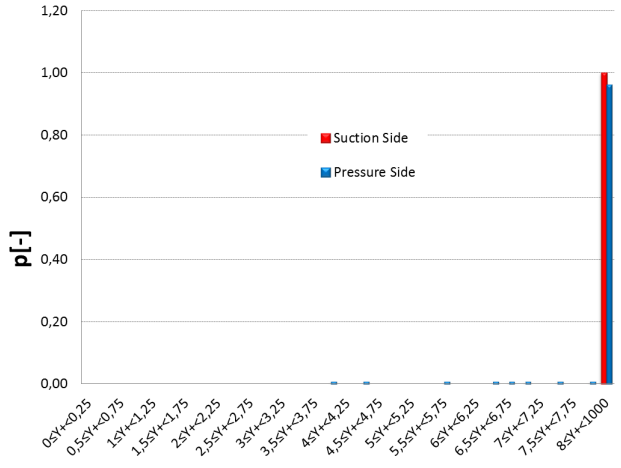

Fig. 13 Graphical representation of the distribution of the y^+ parameter along blade pressure and suction sides; Mod1 mesh, γ-θ Transitional model

Finally, once Mod 3 mesh was identified as the better spatial discretization, the distribution of the skin friction coefficient along both airfoil pressure and suction sides was investigated. Figs. 17 and 18 show a comparison between the numerical predicted skin friction drag using both Spalart-Allmaras turbulence model and γ-θ Transitional model. As can be clearly seen, the Spalart-Allmaras turbulence model is unable to predict the laminar to turbulent transition, which is registered by the γ-θ Transitional model (evidenced by the green arrows) for nearly 35% of chord length.

The registered drag overestimation (+70.6%) of the Spalart-Allmaras turbulence model is connected to the overprediction of the skin friction drag due to a fully turbulent simulation of the flow field close to the airfoil, being the area under the skin friction curve equal to the overall skin friction coefficient. The described phenomenon is quite relevant for the airfoil pressure side, as evidenced by the orange arrows in Fig. 18.

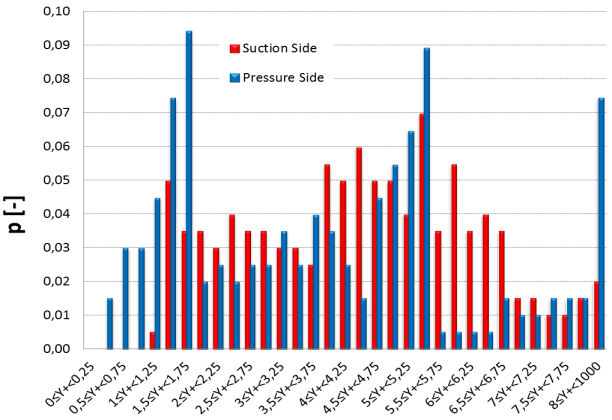

Fig. 14 Graphical representation of the distribution of the y^+ parameter along blade pressure and suction sides; Mod2 mesh, γ-θ Transitional model

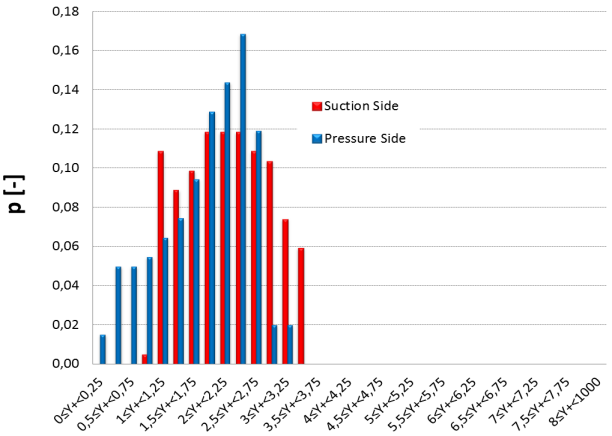

Fig. 15 Graphical representation of the distribution of the y^+ parameter along blade pressure and suction sides; Mod3 mesh, γ-θ Transitional model

VII. Conclusions and Future Works

Laminar to turbulent transition on the DU91-W2-250 airfoil was investigated by means of a CFD simulation of the flow field using the γ-θ Transitional model. Numerical results were compared to both wind tunnel experimental measurements and Spalart-Allmaras turbulence model predictions.

A significant improvement in drag prediction was obtained by using the transitional computation (15.7% overestimation) in comparison with the fully turbulent simulation (70.6% overestimation). The analysis of the distribution of the skin friction coefficient along the airfoil pressure and suction sides confirmed the γ-θ Transitional model capability of foreseeing

the laminar to turbulent transition which, for the present case, was estimated at 35% of the chord length.

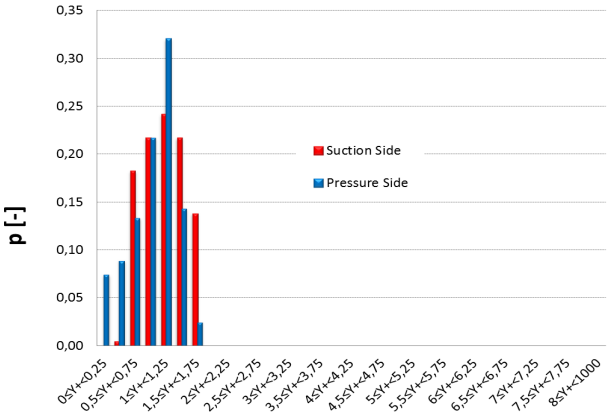

Fig. 16 Graphical representation of the distribution of the y^+ parameter along blade pressure and suction sides; Mod4 mesh, γ-θ Transitional model

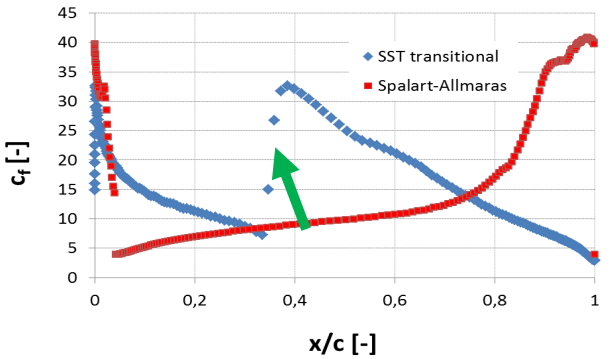

Fig. 17 Numerical predicted skin friction coefficient at suction side for Mod 3 mesh using both Spalart-Allmaras turbulence model and γ-θ Transitional model (the green arrow evidences the point of laminar to turbulent transition onset)

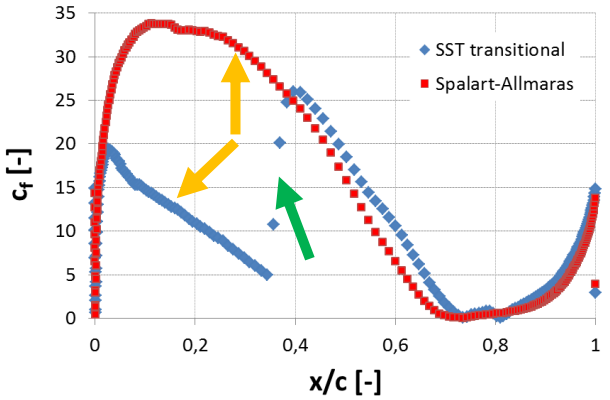

Fig. 18 Numerical predicted skin friction coefficient at pressure side for Mod 3 mesh using both Spalart-Allmaras turbulence model and γ-θ Transitional model (the green arrow evidences the point of laminar to turbulent transition onset, while the orange arrows evidence the deep differences in skin friction drag prediction between Spalart-Allmaras turbulence model and γ-θ Transitional model)

Finally, grid quality was investigated by means of a statistical methodology, obtained by subdividing the global y^+ range in several sub-intervals and computing the probability of the y^+ value at any given point along the airfoil to be comprised inside each sub-interval.

Further work should be performed, in order to extend the present analysis to a wider range of angles of attack.

NOMENCLATURE

c [m]	chord length
C_d [-]	drag coefficient
C_l [-]	lift coefficient
c_f [-]	skin friction coefficient
D [N]	drag force acting on the airfoil
L [N]	lift force acting on the airfoil
P [-]	probability for the y^+ value at any given point along the airfoil to be comprised inside each sub-interval
Re [-]	airfoil Reynolds number
u_τ [m/s]	tangential wall velocity
V_x [m/s]	free-stream wind velocity, x-component
V_y [m/s]	free-stream wind velocity, y-component
V_∞ [m/s]	free-stream wind velocity
x [m]	curvilinear coordinate along airfoil suction/pressure side
X [-]	number of grid elements having the y^+ comprised in the considered interval
y [m]	wall-grid centroid distance
y^+ [-]	wall y-plus
Y [-]	total number of grid elements on airfoil pressure/suction side
α [deg]	airfoil angle of attack
μ [Pa·s]	dynamic viscosity
ρ [kg/m^3]	air density
τ_w [N/m^2]	wall shear stress

REFERENCES

[1] European Wind Energy Association, *EU energy policy after 2020*, www.ewea.org, 2011.

[2] M. Raciti Castelli, G. Grandi and E. Benini, "Numerical Analysis of the Performance of the DU91-W2-250 Airfoil for Straight-Bladed Vertical-Axis Wind Turbine Application", submitted to *ICAFM 2012: International Conference on Advances in Fluid Mechanics*, Florence (Italy), February 28-29, 2012.

[3] W.A. Timmer, W. A. and R. P. J. O. M. van Rooij, "Summary of the delft university wind turbine dedicated airfoils", *AIAA-2003-0352*.

[4] W.A. Timmer, W. A. and R. P. J. O. M. van Rooij, "Design of airfoils for wind turbine blades", *DUWIND, section Wind Energy, Faculty CiTG*, 03 May, 2004.

[5] G. Lombardi, M. V. Salvetti and D. Pinelli, "Numerical Evaluation of Airfoil Friction Drag", *J. Aircraft*, Vol. 37, No. 2, pp. 354-356, 2000.

[6] Y. Lian and W. Shai, "Laminar-Turbulent Transition of a Low Reynolds Number Rigid or Flexible Airfoil", *AIAA Journal*, Vol. 45, No. 7, July 2007, pp. 1501-1513.

[7] F. R. Menter, R. B. Langrty, S. R. Likki, Y. B. Suzen, P. G. Huang and S. Völker, "A Correlation-Based Transition Model Using Local Variables – Part I: Model Formulation", *Journal of Turbomachinery*, Volume 128, Issue 3, pp. 413-422, 2006.

[8] F. R. Menter, R. B. Langrty, S. R. Likki, Y. B. Suzen, P. G. Huang and S. Völker, "A Correlation-Based Transition Model Using Local

Variables – Part II: Test Cases and Industrial Applications", *Journal of Turbomachinery*, Volume 128, Issue 3, pp. 423-434, 2006.

[9] E. Benini and R. Ponza, "Laminar to Turbulent Boundary Layer Transition Investigation on a Supercritical Airfoil Using the γ-θ Transitional Model", *40th Fluid Dynamics Conference and Exhibit*, 28 June – 1 July 2010, Chicago, Illinois, AIAA 2010-4289.

[10] S. Hosseinverdi and M. Boroomand, "Prediction of Laminar-Turbulent Transitional Flow over Single and Two-Element Airfoils", *40th Fluid Dynamics Conference and Exhibit*, 28 June – 1 July 2010, Chicago, Illinois, AIAA 2010-4290.

[11] L. Yuhong and L. Congming, "A numerical simulation of flow around a wind turbine airfoil based on transition model", *WNEC 2009: World Non-Grid-Connected Wind Power and Energy Conference*, Nanjing (China), 24-26 Sept. 2009.

[12] W.A. Timmer, W. A. and R. P. J. O. M. van Rooij, *Aifoil DU91-W2-250 Coordinates and Measurements in Delft University 1.25x1.80 m Low-speed Wind tunnel*, data provided by direct contact from the authors.

[13] ANSYS FLUENT 12.0-12.1 *Documentation*, Release 12.1 © ANSYS, Inc. 2009-10-01.

[14] J. Johansen, "Prediction of Laminar/Turbulent Transition in Airfoil Flows", *Risø National Laboratory*, Roskilde, Denmark, May 1997, Risø-R-987(EN).

[15] M. Raciti Castelli, F. Garbo, E. Benini, "Numerical investigation of laminar to turbulent boundary layer transition on a NACA 0012 airfoil for vertical-axis wind turbine applications", Wind Engineering, Vol. 35, No. 6, 2011, pp. 661-686.